BIOCHEMISTRY
including biophysical chemistry & molecular biology

Current Topic

pubs.acs.org/biochemistry

Cryo-Electron Microscopy and the Amazing Race to Atomic Resolution

Elad Binshtein and Melanie D. Ohi*

Department of Cell and Developmental Biology, Vanderbilt University Medical Center, Nashville, Tennessee 37232, United States

ABSTRACT: Cryo-electron microscopy (cryo-EM), the structural analysis of samples embedded in vitreous ice, is a powerful approach for determining three-dimensional (3D) structures of biological specimens. Over the past two decades, this technique has been used to successfully calculate subnanometer (<10 Å) resolution and, in some cases, near-atomic resolution structures of highly symmetrical and stable complexes such as icosahedral viruses and ribosomes, as well as samples that form ordered two-dimensional or helical arrays. However, determining high-resolution 3D structures of smaller, less symmetrical, and dynamic samples remains a significant challenge. The recent development of electron microscopes with automated data collection capabilities and robust direct electron detection cameras, as well as new powerful image processing algorithms, has dramatically expanded the number of biological macromolecules amenable for study using cryo-EM. In addition, these new technological and computational developments have been used to successfully determine <5 Å resolution 3D structures of samples, such as membrane proteins and complexes with either low or no symmetry, that traditionally were not considered promising candidates for high-resolution cryo-EM. With these exciting new advances, cryo-EM is now on pace to determine atomic resolution 3D structures.

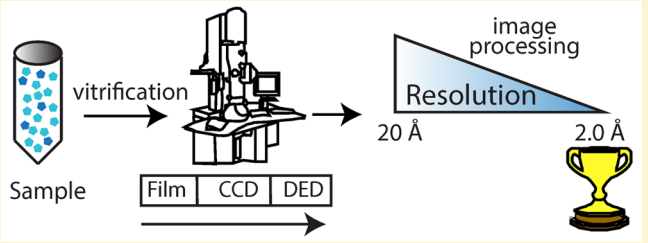

Structural biology strives to determine detailed snapshots of macromolecular machines with the goal of using structure to deduce function. These three-dimensional (3D) molecular models are generated using a range of biophysical techniques, some that generate atomic or near-atomic resolution (from 0.7 to <4 Å) structures, such as X-ray crystallography and nuclear magnetic resonance (NMR), while others, such as small-angle X-ray scattering (SAXS), are useful for generating low-resolution models (>30 Å). The higher the resolution of a structure, the easier it is to uncover how molecular architecture translates into function. While important insights into the overall shape and organization of macromolecules, especially dynamic complexes, can be gained from low- to medium-resolution (30−12 Å) structures, secondary structural elements are only visible in density maps that reach resolutions below 10 Å (Figure 1). For example, α-helices are resolved sub-10 Å resolutions, β-strands are visible at sub-5.0 Å resolutions, and atomic models can start to be built at resolutions below ∼3.5 Å. Until recently, the approaches that consistently yielded atomic resolution structures were X-ray crystallography and NMR spectroscopy; however, new technological and computational developments in the field of cryo-electron microscopy (cryo-EM) have made this rapidly evolving technique a legitimate contender in the race to determine near-atomic resolution 3D structures of biologically important macromolecules that have been difficult to analyze using other structural approaches.

EM is a versatile method for studying biological specimens. In addition to its important history of providing essential information about the subcellular ultrastructures of cells and tissues, the more recently developed molecular EM techniques are used to determine 3D structures of complex macromolecular machines. Molecular EM was developed using the principle that EM images are two-dimensional (2D) projections that contain information about the internal organization of the sample and, thus, can be used to calculate 3D structures.[1−7] Molecular EM methods encompass 2D electron crystallography, helical reconstruction, single-particle analysis, and tomography. In particular, both single-particle EM and tomography have the advantage of not requiring ordered protein arrays. This makes these approaches especially useful for determining structures of biological specimens that are difficult to purify in the large, stable, and homogeneous quantities needed to form ordered crystalline lattices.

Important advances in the theoretical and practical underpinnings of modern molecular EM were developed in the 1970s and early 1980s by researchers such as Richard Henderson and colleagues (2D crystallization[3−5]), David DeRosier and Aaron Klug (helical reconstruction[2,8]), Tony Crowther and colleagues (3D structural calculations of icosahedral viruses[1,9]), Joachim Frank and colleagues (3D structural calculations of asymmetric biological complexes[6,10−12]), Jacques Dubochet and colleagues (vitrifying biological samples[13,14]), and Robert Glaeser and colleagues (imaging vitrified samples[15−17]). However, because the vast majority of 3D structures determined using molecular EM approaches have been at resolutions too low to trace *de novo* individual atoms in the density maps, EM has been yoked with the uninspiring nickname of "blobology".

Received: February 4, 2015
Revised: May 6, 2015
Published: May 8, 2015

DOI: 10.1021/acs.biochem.5b00114
Biochemistry 2015, 54, 3133−3141

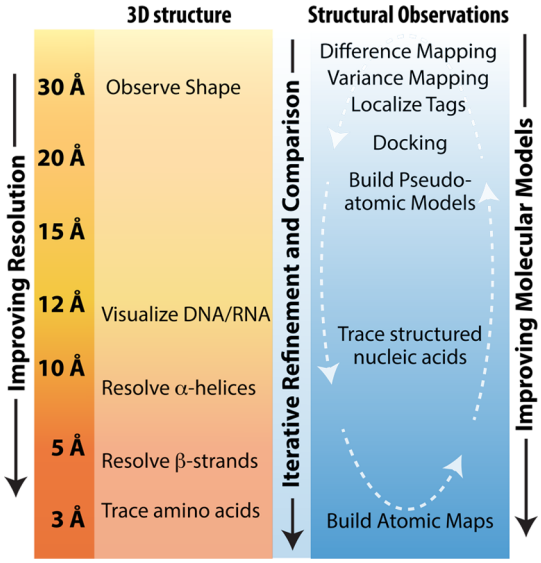

Figure 1. Increasingly detailed molecular models of macromolecules can be generated either by calculating higher-resolution structures or by using a hybrid approach that combines intermediate-resolution structures with other structural, biophysical, biochemical, and/or genetic information. Over the past 20 years, combining molecular EM analysis with hybrid approaches has been successfully used to build pseudoatomic models of structurally challenging cellular machines. However, recent advances in the field of cryo-EM have made it possible to calculate near-atomic resolution structures that can be used to trace the position of individual amino acids in the map.

There are many practical difficulties to overcome upon examination of biological specimens using EM. In general, biological macromolecules scatter electrons poorly, are dehydrated in the microscope vacuum, and accumulate radiation damage, making them challenging specimens for visualization by EM.[17−19] A number of preparative approaches are used to overcome these limitations. For example, 2D crystals are embedded in a sugar-based matrix, and purified complexes are preserved using either negative staining or vitrification. In negative stain EM, protein is adsorbed to a continuous carbon support and then embedded in a layer of a dried heavy metal solution.[20] This technique provides high-contrast structural information and is a powerful preparative approach for analyzing dilute, dynamic samples by single-particle EM. However, the grain size of the stain severely limits the resolution of 3D reconstructions. Further, reconstructions often contain flattening artifacts because the sample is not protected from dehydration in the microscope vacuum. For cryo-EM, the sample is quickly plunged into cryogen, trapping particles in a thin layer of noncubic amorphous, or vitrified ice.[20] Cryo-EM preserves the specimen in a near-native, hydrated environment that protects it from dehydration artifacts. However, unstained samples are sensitive to radiation damage, and the lack of a heavy atom stain leads to low-contrast, noisy images. Although negative stain is a relatively straightforward and simple approach to learn,[21] vitrifying samples and then keeping the ice amorphous as the grid is transferred into the microscope are specialized skills.

The lack of heavy atoms associated with biological samples coupled with the requirement of collecting images using very low electron doses to prevent radiation damage leads to noisy, low-contrast data. The low signal-to-noise ratio (SNR) of cryo-EM images can be partially overcome by aligning and averaging large numbers of collected images of homogeneous particles.

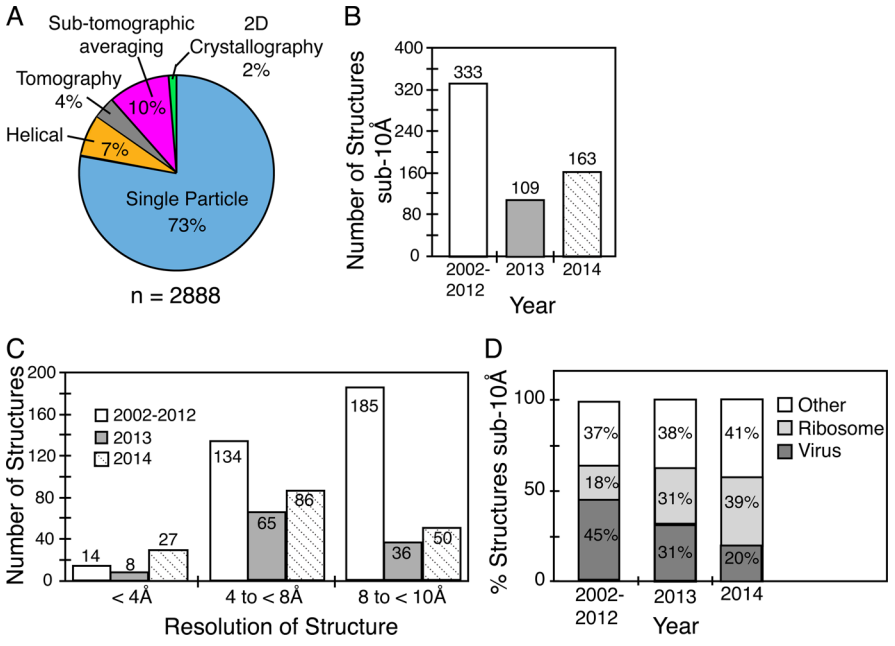

Figure 2. The race to achieve near-atomic resolution structures using cryo-EM has accelerated over the past two years. (A) Pie graph charting the percentage of all structures deposited in the EMDB (Electron Microscopy Data Bank) using various cryo-EM techniques. (B) Bar graph tracking the number of subnanometer (sub-10 Å) single-particle cryo-EM structures deposited in the EMDB over the past 12 years. (C) Bar graph showing the number of sub-4 Å, sub-8 to 4 Å, and sub-10 to 8 Å single-particle cryo-EM structures deposited in the EMDB over the past 12 years. (D) Bar graph showing which percentage of sub-10 Å single-particle cryo-EM structures deposited in the EMDB were of viruses, ribosomes, and other. The majority of the structures listed in the "other" category are of other large symmetrical structures. It is still a challenge to determine high-resolution structures of smaller, dynamic, and/or asymmetric macromolecules.

DOI: 10.1021/acs.biochem.5b00114
Biochemistry 2015, 54, 3133−3141

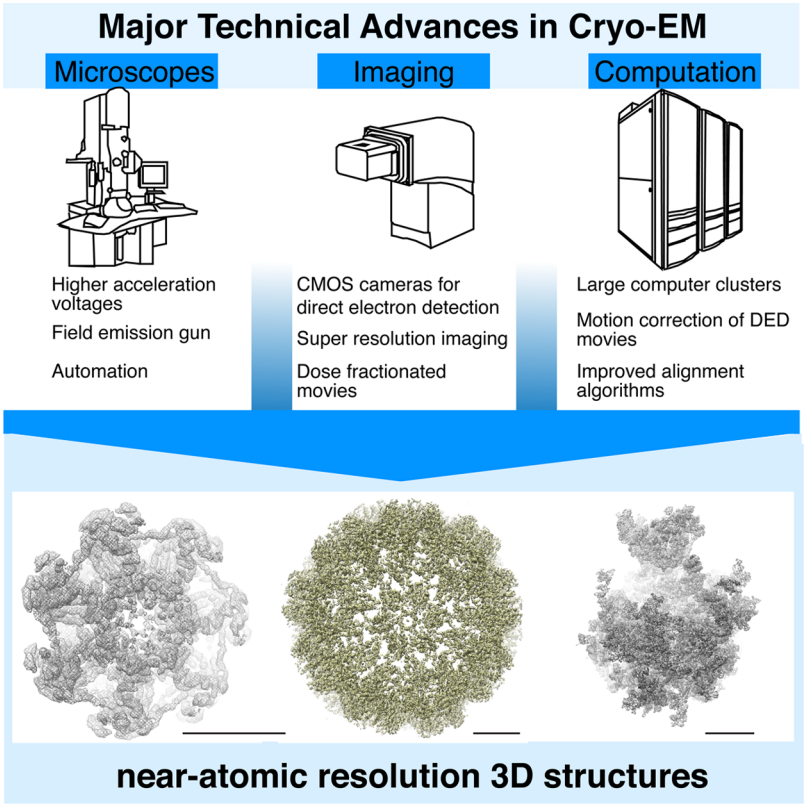

Figure 3. Advances in microscope instrumentation, imaging technology, and computation have driven rapid improvements in the ability to generate near-atomic structures using single-particle cryo-EM. Structures shown from left to right include the 3.3 Å map of the 20S proteasome (EMDB-5623[70]), the 3.8 Å map of the Brome Mosaic Virus (EMDB-6000[107]), and the 3.2 Å map of the yeast mitochondrial large ribosomal subunit (EMDB-2566[83]). All scale bars are 50 Å.

This approach makes it theoretically possible to generate an atomic resolution structure, as was proposed by Richard Henderson as early as 1995.[18] In practice, though, the theoretical promise of generating atomic resolution structures via molecular EM approaches has remained elusive, especially for single-particle EM and tomography. The recent introduction of a group of new technologies and computational approaches has the potential to close this performance gap and propel cryo-EM to the forefront of structural biology's race to answer biological questions at a molecular level. This review focuses on these "game-changing" advances, discussing recent improvements in cryo-EM instrumentation, imaging technologies, and computational approaches.

CRYO-EM TECHNIQUES

The ability to determine 3D structures using cryo-EM relies on either forming ordered 2D crystals (electron crystallography), generating ordered helical assemblies (helical reconstruction), imaging large numbers of homogeneous, randomly oriented particles (single-particle EM), or taking tilt series of thin samples (tomography). In terms of resolution, both electron crystallography and helical reconstruction techniques have the advantage of working with an extended geometrical arrangement of repeating units. Thus, even before the introduction of new imaging and computation technologies, these cryo-EM subdisciplines were used to calculate a number of near-atomic resolution (sub-4 Å) structures (for examples, see refs 22−32). However, coaxing biological samples to organize into repeating arrays remains a challenge. The number of structures found in the Electron Microscopy Data Bank (EMDB) determined using ordered arrays of molecules account for <10% of total deposited structures (Figure 2A).

Both cryo-tomography and single-particle cryo-EM do not require ordered arrays to determine 3D structures, significantly broadening the range of specimens amenable for these analyses. Cryo-tomography is used to examine samples ranging in size from cells to large complexes and often focuses on "one-of-a-kind" objects that are not amenable to averaging methodologies used in single-particle EM. Structures determined using tomography have, until recently, been limited to very low resolutions (>50 Å). While these volumes lack detailed molecular information, the ability to visualize objects in the context of an intact cell at higher resolutions than can be achieved using light microscopy has made tomography an important technique used by cell biologists. However, in cases where multiple copies of a complex or a repeating assembly are found in a tomogram, the use of new electron detectors and subtomographic averaging approaches now makes it possible to use cryo-tomography to determine ∼20−10 Å resolution structures.[33−36] As resolutions of cryo-tomography structures continue to improve, this approach will serve as an important bridge between cell biologists using super-resolution light microscopy techniques and structural biologists.

The most commonly used cryo-EM technique is single-particle EM (Figure 2A), an approach that relies on the ability to collect a large number of images of homogeneous molecules trapped in various orientations in the vitrified ice layer. The goal is to collect a large data set that contains 2D projections of all views of a structurally homogeneous sample. Various computational approaches are then used to convert the 2D

DOI: 10.1021/acs.biochem.5b00114
Biochemistry 2015, 54, 3133−3141

projection information present in the images into a 3D structure.[37−43] The ability to generate a 3D structure requires the accurate determination of five orientation parameters [*x*-axis, *y*-axis, *z*-axis, phi (ψ), and theta (θ)] for each 2D projection, a nontrivial task when relying on images with a low SNR. Thus, despite the theoretical possibility of using single-particle EM to generate atomic resolution maps, until recently many structures never reached subnanometer resolutions. Between the years of 2002 and 2012, only 333 deposited EMDB structures determined using single-particle EM were at sub-10 Å resolution (of a total of 1344, 25%), and of those, only 14 reached near-atomic resolutions (sub-4 Å) (Figure 2B,C). In 2013 alone, there were 109 (of 403, 27%) deposited single-particle cryo-EM structures below 10 Å, with eight reaching sub-4 Å resolution (Figure 2B,C). By 2014, 163 (of 525, 31%) deposited single-particle cryo-EM structures reached sub-10 Å resolutions, with 27 of them at sub-4 Å resolution (Figure 2B,C). In fact, nearly the same number of sub-10 Å structures deposited in the EMDB between 2013 and 2014 was deposited for the entire decade of 2002−2012 (Figure 2B). This trend continues into 2015, with 15 sub-10 Å resolution structures deposited before the end of January, four of these reaching sub-4 Å resolution (only two published at the time of this review[44,45]). Thus, while subnanometer resolution cryo-EM maps were once considered "high-resolution", this designation is quickly becoming reserved only for structures that reach sub-5 Å resolutions.

The acceleration of the use of cryo-EM to determine near-atomic resolution structures can be attributed to improvements in microscopes, imaging technologies, and computational approaches. While these developments promise to continue pushing cryo-EM toward its theoretical potential of reaching atomic resolutions, it is worth noting that ∼60% of the sub-10 Å structures deposited in the EMDB are of viruses and ribosomes (Figure 2D) and nearly all of the deposited sub-4 Å structures are of either viruses, ribosomes, or large symmetrical protein assemblies. Although the gains made in cryo-EM are impressive and should be celebrated for the major technological progress they represent, it remains to be seen whether these high-resolution (sub-5 Å) cryo-EM "wins" will also begin occurring with more regularity when smaller, dynamic, and/or asymmetric macromolecules are being characterized.

IMPROVEMENTS IN CRYO-ELECTRON MICROSCOPES

Since the 1970s, when it was demonstrated that 3D structures could be determined from 2D projections obtained using an electron microscope,[1−7] a steady stream of improvements in electron microscopes has led to large improvements in the ability to generate higher-resolution 3D maps of biological specimens (Figure 3). As a result, electron microscopes are more powerful, stable, reliable, and user-friendly. These advances have significantly improved both the quality of images and the ability of researchers to collect large data sets required to generate 3D structures from noisy 2D projections.

Some of the greatest advances for microscopes have come from the use of higher acceleration voltages (200−300 kV) and a field emission gun (FEG) electron source.[46] These improvements increase both the temporal and spatial coherence of the electron beam, making it possible to collect high-resolution images at the defocus values required to visualize unstained particles in vitrified ice. Although using higher-voltage microscopes can increase image resolution, the improvement in resolution must be balanced with an increased level of sample radiation damage and decreased image contrast.

Other advances in electron microscopes include stable lens systems,[47] improved vacuums, and stable cryo-stages that minimize sample drift. A well-aligned modern cryo-electron microscope can achieve sub-2 Å resolutions when radiation resistant specimens are being examined. However, biological samples are easily damaged in the electron beam, requiring a delicate balance between applying a sufficiently large electron dose to detect signal while not destroying the structural integrity of the sample. In practice, this means that images of biological samples will have a low SNR, making it essential to collect data sets containing thousands to hundreds of thousands of particles, depending on whether the sample is large and highly symmetrical or dynamic and asymmetrical, respectively.

Modern electron microscopes are also fully computerized, leading to the development and integration of software that increases the efficiency of data collection. One important advance has been the digital integration of "low-dose mode", a protocol developed in the 1970s to reduce the level of radiation damage to biological samples during data collection.[5,48−50] Working in this setting on a computerized microscope makes it straightforward to collect precisely defocused images using a minimal electron dose. Another important software advance is the ability to fully automate image collection via control of a computerized stage. A number of academic and commercial programs have been developed that allow users to quickly scan grids for appropriate regions of vitrified ice and then collect images with minimal intervention from the microscope operator.[51−55] The use of these programs has significantly improved the ability to efficiently collect large amounts of high-quality data in the most efficient manner.

IMPROVEMENTS IN IMAGING TECHNOLOGIES

The susceptibility of biological samples to radiation damage limits the electron dose that can be used to generate images, making detector technology an important area of development for cryo-EM. The type of detector used to collect cryo-EM images profoundly influences data quality and the ability to determine high-resolution structures. Detector performance is measured by two parameters: the modulation transfer function (MTF) and the detective quantum efficiency (DQE). The MTF quantifies the response of the detector at various frequencies (i.e., the resolution of the camera), while the DQE quantifies the combined effects of the signal generated by the sample and the noise generated by the camera in the final image. Using these parameters, the ideal imaging device would have a high MTF across the spectrum and generate images using only the signal arising from the sample with no added noise from the detector. Unfortunately, this perfect detector does not yet exist, which means all detectors have resolution limits and contribute varying levels of noise to the final image.

Historically, film cameras, with a DQE of ∼0.3 and the ability to take images of a relatively large area of the grid, were the favored detector for collecting cryo-EM images.[56] In fact, nine of the 14 sub-4 Å structures deposited in the EMDB between 2002 and 2012 were determined using images collected on film (Figure 2C).[57−64] In addition, film was used to collect the images used to calculate the impressive 3.3 Å structure of an icosahedral virus.[65] However, drawbacks of using film include the labor-intensive and time-consuming requirements of developing the film and then scanning the negatives into a digital format, processes that significantly expanded the time

DOI: 10.1021/acs.biochem.5b00114
Biochemistry 2015, 54, 3133−3141

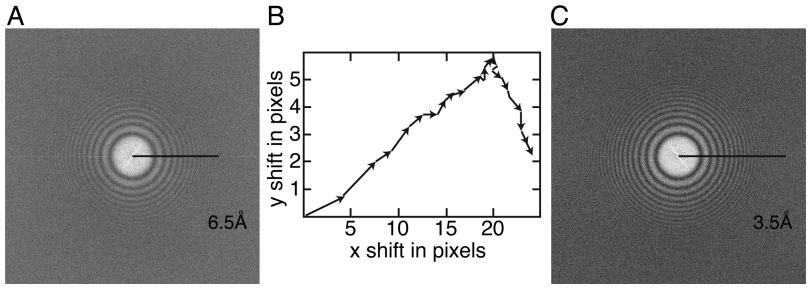

Figure 4. Motion correction of dose-fractionated movies taken using a DED camera improves resolution and quality of cryo-EM images. (A) Power spectra of a summed, but not motion-corrected, 30 image dose-fractionated stack of the *Helicobacter pylori* toxin VacA in vitrified ice. Stacks were taken using a Gatan K2 Summit DED camera in super-resolution mode. The highest visible Thon ring is at 6.5 Å. (B) Graph of the calculated shifts used for motion correction. The algorithm was developed by Li et al.[70] (C) Power spectra of the motion-corrected and summed image. The highest visible Thon ring is now at 3.5 Å resolution.

needed for data collection and limited the ability to use automated data collection. Because of these drawbacks, alternative imaging technologies have been developed. One popular alternative to film is charge-coupled device (CCD) cameras. Although the efficiency of CCD cameras (DQE ~ 0.1) does not rival film, the ability to integrate them with automated data collection software makes it possible to use these detectors to collect images over an extended data collection session.[66,67]

The newest innovation in EM imaging technology is the development of a direct electron detection (DED) camera that records images directly on a sensor, rather than digitizing the signal from electrons through the coupling of a scintillator and fiber-optics as is found in CCD devices (Figure 3). DED cameras are made of a thin semiconductor membrane directly connected to a thin matrix. The thickness of the supporting matrix is important because thinner matrices generate less noise from backscattered electrons.[68] The performance of back-thinned DED cameras exceeds that of film while remaining amenable to automation.[69−71]

At sufficiently low electron doses, DED cameras can detect individual electrons, substantially improving the SNR of an image.[72] However, the low-dose exposures commonly used to collect cryo-EM images saturate the DED sensor. To overcome this limitation and generate the highest-resolution images, DED cameras are run in a "movie mode" that fractionates the electron dose across a long exposure (~6 s) that is recorded at a rapid frame rate (0.2 s/frame). The end result is that each imaging event is a collection of ~20−30 individual very low-contrast images that must be combined before any further image processing and structural calculations can be implemented. In addition to improving the resolution of the images, the use of DED cameras to collect cryo-EM "movies" has had profound effects on how data are chosen and used in image processing, a topic that will be further discussed in the next section. The development of robust and commercial DED cameras is the most groundbreaking advance in cryo-EM over the past five years, and this technology has quickly become an essential requirement for cryo-EM facilities.

■ IMPROVEMENTS IN COMPUTATION

Converting large data sets of 2D projections into a 3D structure requires algorithms that can accurately determine the position and orientation of the imaged particles, a process that requires significant computational power. Conveniently for cryo-EM, large computer clusters have become increasingly available, as well as more powerful, over the past decade. These resources allow large computational jobs, such as the alignment and classification of thousands to hundreds of thousands of noisy 2D projections, to be run in parallel on multiple computer processors, a strategy that significantly reduces the amount of time required to turn raw images into 3D structures. Additionally, these rapidly evolving computational resources have made it possible for computationally intensive image processing algorithms to be employed for structural calculations (Figure 3). Image processing is required to both correct for particle movement within the vitrified ice layer and precisely classify the orientation of 2D projections. The development of faster computational resources combined with new image processing strategies has led to the ability to calculate more detailed structural models from noisy cryo-EM images.

The collection of cryo-EM images in "movie mode" allows for the tracking of beam-induced movement of both the vitrified ice layer and the embedded particles.[73,74] This movement causes blurring of the final image, limiting the ability to generate high-resolution structures. A number of algorithms that correct for this beam-induced motion have now been developed. These approaches align the individual dose-fractionated images, either using the entire image or the individually windowed particles, before summing the frames into a final image.[70,75−77] This procedure significantly improves the quality of the final data for two reasons (Figure 4). First, the alignment algorithms correct the beam-induced motion, and second, the effects of radiation damage can be reduced by carefully choosing which dose-fractionated images are included in the final summed image.[76,78]

Improvements in algorithms have also made it possible to analyze data sets that contain some structural heterogeneity. Macromolecules undergo varying levels of dynamic movement as part of their biological function. For this reason, even biochemically pure samples are rarely structurally homogeneous, with specimens naturally adopting more than one conformation in vitrified ice. In the ideal situation, molecules are found in various orientations in the amorphous ice layer providing many different views of the molecule. While different views of the molecules are necessary for accurate structural calculations, they can create serious problems during 3D reconstruction if the purified sample is either compositionally or structurally heterogeneous. To determine a high-resolution 3D structure, only images of structurally identical molecules should be included in the reconstruction. However, from projection views alone, it can be difficult to distinguish between particles in different orientations and particles that are in different conformational states. The more heterogeneous the sample, the more difficult this problem becomes. Numerous

DOI: 10.1021/acs.biochem.5b00114
Biochemistry 2015, 54, 3133−3141

image processing approaches have been developed to precisely assign orientation parameters to 2D projections and ensure projections of only structurally homogeneous particles are included in a 3D reconstruction. Common program suites used for image processing of single-particle cryo-EM data include SPIDER, Xmipp, EMAN2, SPARX, FREALIGN, and RELION.[38−43] These programs all use different classification and 3D reconstruction strategies, giving them distinct strengths and weaknesses that are beyond the scope of this review. However, because of these differences, it is common for multiple programs to be used at different stages of the classification, 3D reconstruction, and refinement processes (for examples, see refs 79 and 80). Both FREALIGN,[38] a program that uses a partial implementation of the maximum-likelihood approach, and RELION,[42] a program that adds Bayesian analysis to the maximum-likelihood approach, deserve a special mention because these programs, in combination with motion correction algorithms, have been used to determine a number of high-resolution (sub-5 Å) structures (some examples include refs 70, 74, and 80−91). The ability of cryo-EM to classify structurally diverse data sets, sometimes termed *in silico* purification, makes single-particle EM a powerful method for determining structures of many biologically essential complexes that are difficult to crystallize because of their inherent conformational heterogeneity. However, at this time, the image processing algorithms are still limited by the amount of structural heterogeneity that can be tolerated. As mentioned previously, a majority of high-resolution structures deposited in the EMDB are of ribosomes, icosahedral viruses, and large symmetrical specimens (Figure 2D). Classifying smaller, asymmetric, and/or highly dynamic samples remains a significant challenge.

WHAT ARE THE NEXT CHALLENGES IN THE QUICKLY ADVANCING FIELD OF CRYO-EM?

Twenty years after Richard Henderson's original predictions,[18] cryo-EM is finally poised to begin performing up to its theoretical promise of generating atomic resolution 3D structures. The synergistic progress made in instrumentation, DED cameras, and computational approaches has led to astonishing advances in the ability of single-particle cryo-EM to determine near-atomic resolution structures (Figure 3). However, instead of resting on its laurels, the field continues to work toward the goal of determining sub-3 Å structures, as well as expanding the types of samples that are amenable to high-resolution (sub-5 Å) structure determination.

Although the majority of sub-5 Å structures continue to be of large, relatively rigid complexes (Figure 2D), the 4.5 Å map of the small (∼230 kDa), membrane protein complex γ-secretase[87] (Figure 5A) and the 3.4 Å structure of the 4-fold symmetrical mammalian TRPV1 (transient receptor potential vanilloid) membrane channel[86] (Figure 5B) are the first, of what is hoped to be many, high-resolution structures of challenging samples that would not have been amenable for structural analysis by cryo-EM without these new technological advances. Areas of active research that continue to push the boundaries of cryo-EM include further development in automated data collection strategies (e.g., refs 92−94), the continued improvement of DED cameras, the use of phase plates for in-focus phase contrast (e.g., refs 95−97), the development of new grid substrates to reduce beam-induced sample motion (e.g., refs 98 and 99), and new classification algorithms to expand the capability of *in silico* purification (e.g., refs 100−102). In addition, as increasing numbers of cryo-EM

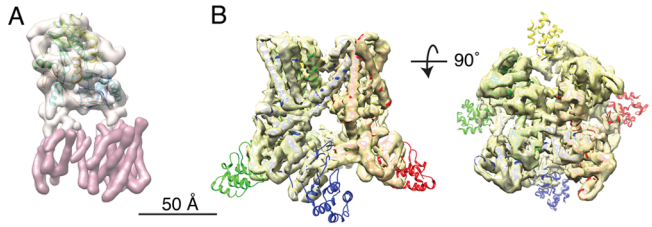

Figure 5. Synergy of cryo-EM technical advances has led to the determination of high-resolution structures (sub-5 Å) of challenging samples. (A) The 4.5 Å structure of the ∼230 kDa membrane protein complex γ-secretase (EMD-2677, PDB entry 4UPC).[87] Images were collected on a K2 Summit DED camera and the structure calculated using RELION.[42] The transmembrane segments are colored pink, while the extracellular domains are colored tan. (B) Structure of the 4-fold symmetrical mammalian TRPV1 membrane channel at 3.3 Å resolution (EMD-5778, PDB entry 3J5P).[86] Images were collected on a K2 Summit DED camera, and the structure was calculated using RELION.[42] The EM density is colored yellow, while atomic models of the four identical TRPV1 subunits are colored blue, green, yellow, and red. The TRPV1 atomic models were partially built using the cryo-EM map. A portion of the TRPV1 ankyrin repeats found outside the density map were not observed in the EM structure, likely because of their flexibility. The structure is rotated 90° on its *x*-axis. The scale bar in each panel is 50 Å.

structures reach near-atomic resolution, new tools are needed for building atomic models using EM density maps and for verifying the quality of high-resolution structures.

Finally, even with these technological advances, not all cryo-EM structures will reach the new high-resolution threshold of sub-5 Å that has been established by studies of large, stable complexes (Figure 2D). The lack of compositional and structural homogeneity of samples used in cryo-EM remains a major limiting factor for generating high-resolution structures. Unfortunately, there are no shortcuts for improving sample quality, and this step often remains a labor-intensive iterative process that can require optimization for months to years before the purification is amenable for structural analysis. In addition, there are essential biological machines that are intrinsically dynamic. Even when purified to homogeneity, these dynamic macromolecules will remain structurally heterogeneous. For these reasons, low- to medium-resolution cryo-EM structures (30−8 Å) are still critical for providing insights into the organization and function of many challenging biological samples that cannot be visualized using alternative techniques. One of cryo-EM's earliest successes came from the structural characterization of the ribosome, even though these structures would now be considered low-resolution. Long before near-atomic resolution structures were on the horizon, these "blobby" 3D maps of the ribosome provided crucial molecular insight, clarifying the individual contributions made by both ribosomal RNA and protein components during protein synthesis (reviewed in refs 103−106). In the exhilarating pursuit of achieving near-atomic and atomic resolution structures, it is important for cryo-EM as a field to not lose perspective that the overarching goal of structural biology is to answer biological questions. Although high-resolution structures are beautiful and fun to work with, the fact remains that answers to many basic questions do not require atomic resolution information, especially when molecular EM analysis is combined with proteomic, genetic, and biochemical studies.

DOI: 10.1021/acs.biochem.5b00114
Biochemistry 2015, 54, 3133−3141

AUTHOR INFORMATION

Corresponding Author

*Department of Cell and Developmental Biology, Vanderbilt University Medical School, Room 4160A, MRBIII, 465 21st Ave., South Nashville, TN 37232-8240. E-mail: Melanie.ohi@vanderbilt.edu. Phone: (615) 936-7780.

Notes

The authors declare no competing financial interest.

ACKNOWLEDGMENTS

We thank members of the Ohi lab and Kathleen Mittendorf for helpful comments and suggestions.

ABBREVIATIONS

cryo-EM, cryo-electron microscopy; DQE, detective quantum efficiency; EM, electron microscopy; EMDB, Electron Microscopy Data Bank; DED, direct electron detection; FEG, field emission gun; MTF, modulation transfer function; NMR, nuclear magnetic resonance; SAXS, small-angle X-ray scattering; SNR, signal-to-noise ratio; 3D, three-dimensional; 2D, two-dimensional; PDB, Protein Data Bank.

REFERENCES

(1) Crowther, R. A., Amos, L. A., Finch, J. T., De Rosier, D. J., and Klug, A. (1970) Three dimensional reconstructions of spherical viruses by fourier synthesis from electron micrographs. *Nature 226*, 421−425.

(2) DeRosier, D. J., and Klug, A. (1972) Structure of the tubular variants of the head of bacteriophage T4 (polyheads). I. Arrangement of subunits in some classes of polyheads. *J. Mol. Biol. 65*, 469−488.

(3) Henderson, R., and Unwin, P. N. (1975) Three-dimensional model of purple membrane obtained by electron microscopy. *Nature 257*, 28−32.

(4) Henderson, R., and Unwin, P. N. (1977) Structure of the purple membrane from *Halobacterium halobium*. *Biophys. Struct. Mech. 3*, 121.

(5) Unwin, P. N., and Henderson, R. (1975) Molecular structure determination by electron microscopy of unstained crystalline specimens. *J. Mol. Biol. 94*, 425−440.

(6) Frank, J., Goldfarb, W., Eisenberg, D., and Baker, T. S. (1978) Reconstruction of glutamine synthetase using computer averaging. *Ultramicroscopy 3*, 283−290.

(7) Hayward, S. B., and Glaeser, R. M. (1979) Radiation damage of purple membrane at low temperature. *Ultramicroscopy 04*, 201−210.

(8) De Rosier, D. J., and Klug, A. (1968) Reconstruction of three dimensional structures from electron micrographs. *Nature 217*, 130−134.

(9) Crowther, R. A. (1971) Procedures for three-dimensional reconstruction of spherical viruses by Fourier synthesis from electron micrographs. *Philos. Trans. R. Soc., B 261*, 221−230.

(10) Frank, J., Verschoor, A., and Boublik, M. (1981) Computer averaging of electron micrographs of 40S ribosomal subunits. *Science 214*, 1353−1355.

(11) Verschoor, A., Frank, J., Radermacher, M., Wagenknecht, T., and Boublik, M. (1984) Three-dimensional reconstruction of the 30 S ribosomal subunit from randomly oriented particles. *J. Mol. Biol. 178*, 677−698.

(12) Radermacher, M., and Frank, J. (1984) Representation of three-dimensionally reconstructed objects in electron microscopy by surfaces of equal density. *J. Microsc. (Oxford, U.K.) 136*, 77−85.

(13) Adrian, M., Dubochet, J., Lepault, J., and McDowall, A. W. (1984) Cryo-electron microscopy of viruses. *Nature 308*, 32−36.

(14) Dubochet, J., Booy, F. P., Freeman, R., Jones, A. V., and Walter, C. A. (1981) Low temperature electron microscopy. *Annu. Rev. Biophys. Bioeng. 10*, 133−149.

(15) Taylor, K. A., and Glaeser, R. M. (1974) Electron diffraction of frozen, hydrated protein crystals. *Science 186*, 1036−1037.

(16) Kuo, I. A., and Glaeser, R. M. (1975) Development of methodology for low exposure, high resolution electron microscopy of biological specimens. *Ultramicroscopy 1*, 53−66.

(17) Glaeser, R. M., and Taylor, K. A. (1978) Radiation damage relative to transmission electron microscopy of biological specimens at low temperature: A review. *J. Microsc. (Oxford, U.K.) 112*, 127−138.

(18) Henderson, R. (1995) The potential and limitations of neutrons, electrons and X-rays for atomic resolution microscopy of unstained biological molecules. *Q. Rev. Biophys. 28*, 171−193.

(19) Glaeser, R. M., and Hall, R. J. (2011) Reaching the information limit in cryo-EM of biological macromolecules: Experimental aspects. *Biophys. J. 100*, 2331−2337.

(20) Ohi, M. D. (2009) EM analysis of protein structure: Negative staining, rotary shadowing, and cryoEM. *Encyclopedia of Life Sciences*, Wiley-Blackwell, New York.

(21) Ohi, M., Li, Y., Cheng, Y., and Walz, T. (2004) Negative Staining and Image Classification: Powerful Tools in Modern Electron Microscopy. *Biol. Proced. Online 6*, 23−34.

(22) Henderson, R., Baldwin, J. M., Ceska, T. A., Zemlin, F., Beckmann, E., and Downing, K. H. (1990) Model for the structure of bacteriorhodopsin based on high-resolution electron cryo-microscopy. *J. Mol. Biol. 213*, 899−929.

(23) Kuhlbrandt, W., Wang, D. N., and Fujiyoshi, Y. (1994) Atomic model of plant light-harvesting complex by electron crystallography. *Nature 367*, 614−621.

(24) Kimura, Y., Vassylyev, D. G., Miyazawa, A., Kidera, A., Matsushima, M., Mitsuoka, K., Murata, K., Hirai, T., and Fujiyoshi, Y. (1997) Surface of bacteriorhodopsin revealed by high-resolution electron crystallography. *Nature 389*, 206−211.

(25) Nogales, E., Wolf, S. G., and Downing, K. H. (1998) Structure of the $\alpha\beta$ tubulin dimer by electron crystallography. *Nature 391*, 199−203.

(26) Murata, K., Mitsuoka, K., Hirai, T., Walz, T., Agre, P., Heymann, J. B., Engel, A., and Fujiyoshi, Y. (2000) Structural determinants of water permeation through aquaporin-1. *Nature 407*, 599−605.

(27) Mitra, A. K., Ren, G., Reddy, V. S., Cheng, A., and Froger, A. (2002) The architecture of a water-selective pore in the lipid bilayer visualized by electron crystallography in vitreous ice. *Novartis Found. Symp. 245*, 33−46 , 46−50 (discussion), 165−168.

(28) Miyazawa, A., Fujiyoshi, Y., and Unwin, N. (2003) Structure and gating mechanism of the acetylcholine receptor pore. *Nature 423*, 949−955.

(29) Yonekura, K., Maki-Yonekura, S., and Namba, K. (2003) Complete atomic model of the bacterial flagellar filament by electron cryomicroscopy. *Nature 424*, 643−650.

(30) Gonen, T., Sliz, P., Kistler, J., Cheng, Y., and Walz, T. (2004) Aquaporin-0 membrane junctions reveal the structure of a closed water pore. *Nature 429*, 193−197.

(31) Maki-Yonekura, S., Yonekura, K., and Namba, K. (2010) Conformational change of flagellin for polymorphic supercoiling of the flagellar filament. *Nat. Struct. Mol. Biol. 17*, 417−422.

(32) Ge, P., and Zhou, Z. H. (2011) Hydrogen-bonding networks and RNA bases revealed by cryo electron microscopy suggest a triggering mechanism for calcium switches. *Proc. Natl. Acad. Sci. U.S.A. 108*, 9637−9642.

(33) Tran, E. E., Borgnia, M. J., Kuybeda, O., Schauder, D. M., Bartesaghi, A., Frank, G. A., Sapiro, G., Milne, J. L., and Subramaniam, S. (2012) Structural mechanism of trimeric HIV-1 envelope glycoprotein activation. *PLoS Pathog. 8*, e1002797.

(34) Bartesaghi, A., Lecumberry, F., Sapiro, G., and Subramaniam, S. (2012) Protein secondary structure determination by constrained single-particle cryo-electron tomography. *Structure 20*, 2003−2013.

(35) Schur, F. K., Hagen, W. J., de Marco, A., and Briggs, J. A. (2013) Determination of protein structure at 8.5 Å resolution using cryo-electron tomography and sub-tomogram averaging. *J. Struct. Biol. 184*, 394−400.

(36) Schur, F. K., Hagen, W. J., Rumlova, M., Ruml, T., Muller, B., Krausslich, H. G., and Briggs, J. A. (2015) Structure of the immature

DOI: 10.1021/acs.biochem.5b00114
Biochemistry 2015, 54, 3133−3141

HIV-1 capsid in intact virus particles at 8.8 Å resolution. *Nature 517*, 505−508.
(37) van Heel, M., Harauz, G., Orlova, E. V., Schmidt, R., and Schatz, M. (1996) A new generation of the IMAGIC image processing system. *J. Struct. Biol. 116*, 17−24.
(38) Grigorieff, N. (2007) FREALIGN: High-resolution refinement of single particle structures. *J. Struct. Biol. 157*, 117−125.
(39) Hohn, M., Tang, G., Goodyear, G., Baldwin, P. R., Huang, Z., Penczek, P. A., Yang, C., Glaeser, R. M., Adams, P. D., and Ludtke, S. J. (2007) SPARX, a new environment for Cryo-EM image processing. *J. Struct. Biol. 157*, 47−55.
(40) Tang, G., Peng, L., Baldwin, P. R., Mann, D. S., Jiang, W., Rees, I., and Ludtke, S. J. (2007) EMAN2: An extensible image processing suite for electron microscopy. *J. Struct. Biol. 157*, 38−46.
(41) Shaikh, T. R., Gao, H., Baxter, W. T., Asturias, F. J., Boisset, N., Leith, A., and Frank, J. (2008) SPIDER image processing for single-particle reconstruction of biological macromolecules from electron micrographs. *Nat. Protoc. 3*, 1941−1974.
(42) Scheres, S. H. (2012) RELION: Implementation of a Bayesian approach to cryo-EM structure determination. *J. Struct. Biol. 180*, 519−530.
(43) de la Rosa-Trevin, J. M., Oton, J., Marabini, R., Zaldivar, A., Vargas, J., Carazo, J. M., and Sorzano, C. O. (2013) Xmipp 3.0: An improved software suite for image processing in electron microscopy. *J. Struct. Biol. 184*, 321−328.
(44) Shao, S., Brown, A., Santhanam, B., and Hegde, R. S. (2015) Structure and Assembly Pathway of the Ribosome Quality Control Complex. *Mol. Cell 57*, 433−444.
(45) Shen, P. S., Park, J., Qin, Y., Li, X., Parsawar, K., Larson, M. H., Cox, J., Cheng, Y., Lambowitz, A. M., Weissman, J. S., Brandman, O., and Frost, A. (2015) Protein synthesis. Rqc2p and 60S ribosomal subunits mediate mRNA-independent elongation of nascent chains. *Science 347*, 75−78.
(46) Zhou, Z. H., and Chiu, W. (1993) Prospects for using an IVEM with a FEG for imaging macromolecules towards atomic resolution. *Ultramicroscopy 49*, 407−416.
(47) Glaeser, R. M., Typke, D., Tiemeijer, P. C., Pulokas, J., and Cheng, A. (2011) Precise beam-tilt alignment and collimation are required to minimize the phase error associated with coma in high-resolution cryo-EM. *J. Struct. Biol. 174*, 1−10.
(48) Williams, R. C., and Fisher, H. W. (1970) Electron microscopy of tobacco mosaic virus under conditions of minimal beam exposure. *J. Mol. Biol. 52*, 121−123.
(49) Ohtsuki, M., and Zeitler, E. (1975) Minimal beam exposure with a field emission source. *Ultramicroscopy 1*, 163−165.
(50) Fujiyoshi, Y., Kobayashi, T., Ishizuka, K., Uyeda, N., Ishida, Y., and Harada, Y. (1980) A new method for the optimal-resolutoin electron microscopy of radiation-sensitive specimens. *Ultramicroscopy 5*, 459−468.
(51) Zhang, P., Borgnia, M. J., Mooney, P., Shi, D., Pan, M., O'Herron, P., Mao, A., Brogan, D., Milne, J. L., and Subramaniam, S. (2003) Automated image acquisition and processing using a new generation of 4K × 4K CCD cameras for cryo electron microscopic studies of macromolecular assemblies. *J. Struct. Biol. 143*, 135−144.
(52) Mastronarde, D. N. (2005) Automated electron microscope tomography using robust prediction of specimen movements. *J. Struct. Biol. 152*, 36−51.
(53) Lei, J., and Frank, J. (2005) Automated acquisition of cryo-electron micrographs for single particle reconstruction on an FEI Tecnai electron microscope. *J. Struct. Biol. 150*, 69−80.
(54) Suloway, C., Pulokas, J., Fellmann, D., Cheng, A., Guerra, F., Quispe, J., Stagg, S., Potter, C. S., and Carragher, B. (2005) Automated molecular microscopy: The new Leginon system. *J. Struct. Biol. 151*, 41−60.
(55) Suloway, C., Shi, J., Cheng, A., Pulokas, J., Carragher, B., Potter, C. S., Zheng, S. Q., Agard, D. A., and Jensen, G. J. (2009) Fully automated, sequential tilt-series acquisition with Leginon. *J. Struct. Biol. 167*, 11−18.
(56) McMullan, G., Chen, S., Henderson, R., and Faruqi, A. R. (2009) Detective quantum efficiency of electron area detectors in electron microscopy. *Ultramicroscopy 109*, 1126−1143.
(57) Zhang, X., Settembre, E., Xu, C., Dormitzer, P. R., Bellamy, R., Harrison, S. C., and Grigorieff, N. (2008) Near-atomic resolution using electron cryomicroscopy and single-particle reconstruction. *Proc. Natl. Acad. Sci. U.S.A. 105*, 1867−1872.
(58) Yu, X., Ge, P., Jiang, J., Atanasov, I., and Zhou, Z. H. (2011) Atomic model of CPV reveals the mechanism used by this single-shelled virus to economically carry out functions conserved in multishelled reoviruses. *Structure 19*, 652−661.
(59) Wolf, M., Garcea, R. L., Grigorieff, N., and Harrison, S. C. (2010) Subunit interactions in bovine papillomavirus. *Proc. Natl. Acad. Sci. U.S.A. 107*, 6298−6303.
(60) Zhang, X., Sun, S., Xiang, Y., Wong, J., Klose, T., Raoult, D., and Rossmann, M. G. (2012) Structure of Sputnik, a virophage, at 3.5-Å resolution. *Proc. Natl. Acad. Sci. U.S.A. 109*, 18431−18436.
(61) Liu, H., Jin, L., Koh, S. B., Atanasov, I., Schein, S., Wu, L., and Zhou, Z. H. (2010) Atomic structure of human adenovirus by cryo-EM reveals interactions among protein networks. *Science 329*, 1038−1043.
(62) Estrozi, L. F., and Navaza, J. (2010) Ab initio high-resolution single-particle 3D reconstructions: The symmetry adapted functions way. *J. Struct. Biol. 172*, 253−260.
(63) Settembre, E. C., Chen, J. Z., Dormitzer, P. R., Grigorieff, N., and Harrison, S. C. (2011) Atomic model of an infectious rotavirus particle. *EMBO J. 30*, 408−416.
(64) Chen, D. H., Baker, M. L., Hryc, C. F., DiMaio, F., Jakana, J., Wu, W., Dougherty, M., Haase-Pettingell, C., Schmid, M. F., Jiang, W., Baker, D., King, J. A., and Chiu, W. (2011) Structural basis for scaffolding-mediated assembly and maturation of a dsDNA virus. *Proc. Natl. Acad. Sci. U.S.A. 108*, 1355−1360.
(65) Zhang, X., Jin, L., Fang, Q., Hui, W. H., and Zhou, Z. H. (2010) 3.3 Å cryo-EM structure of a nonenveloped virus reveals a priming mechanism for cell entry. *Cell 141*, 472−482.
(66) Faruqi, A. R. (1998) Design principles and applications of a cooled CCD camera for electron microscopy. *Adv. Exp. Med. Biol. 453*, 63−72.
(67) Sander, B., Golas, M. M., and Stark, H. (2005) Advantages of CCD detectors for de novo three-dimensional structure determination in single-particle electron microscopy. *J. Struct. Biol. 151*, 92−105.
(68) McMullan, G., Faruqi, A. R., Henderson, R., Guerrini, N., Turchetta, R., Jacobs, A., and van Hoften, G. (2009) Experimental observation of the improvement in MTF from backthinning a CMOS direct electron detector. *Ultramicroscopy 109*, 1144−1147.
(69) Ruskin, R. S., Yu, Z., and Grigorieff, N. (2013) Quantitative characterization of electron detectors for transmission electron microscopy. *J. Struct. Biol. 184*, 385−393.
(70) Li, X., Mooney, P., Zheng, S., Booth, C. R., Braunfeld, M. B., Gubbens, S., Agard, D. A., and Cheng, Y. (2013) Electron counting and beam-induced motion correction enable near-atomic-resolution single-particle cryo-EM. *Nat. Methods 10*, 584−590.
(71) McMullan, G., Faruqi, A. R., Clare, D., and Henderson, R. (2014) Comparison of optimal performance at 300 keV of three direct electron detectors for use in low dose electron microscopy. *Ultramicroscopy 147*, 156−163.
(72) McMullan, G., Clark, A. T., Turchetta, R., and Faruqi, A. R. (2009) Enhanced imaging in low dose electron microscopy using electron counting. *Ultramicroscopy 109*, 1411−1416.
(73) Brilot, A. F., Chen, J. Z., Cheng, A., Pan, J., Harrison, S. C., Potter, C. S., Carragher, B., Henderson, R., and Grigorieff, N. (2012) Beam-induced motion of vitrified specimen on holey carbon film. *J. Struct. Biol. 177*, 630−637.
(74) Campbell, M. G., Cheng, A., Brilot, A. F., Moeller, A., Lyumkis, D., Veesler, D., Pan, J., Harrison, S. C., Potter, C. S., Carragher, B., and Grigorieff, N. (2012) Movies of ice-embedded particles enhance resolution in electron cryo-microscopy. *Structure 20*, 1823−1828.

DOI: 10.1021/acs.biochem.5b00114
Biochemistry 2015, 54, 3133−3141

(75) Shigematsu, H., and Sigworth, F. J. (2013) Noise models and cryo-EM drift correction with a direct-electron camera. *Ultramicroscopy 131*, 61−69.
(76) Scheres, S. H. (2014) Beam-induced motion correction for sub-megadalton cryo-EM particles. *eLife 3*, e03665.
(77) Rubinstein, J. L., and Brubaker, M. A. (2014) Alignment of cryo-EM movies of individual particles by global optimization of image translations. *arXiv*, 1409.6789.
(78) Baker, L. A., and Rubinstein, J. L. (2010) Radiation damage in electron cryomicroscopy. *Methods Enzymol. 481*, 371−388.
(79) Greber, B. J., Boehringer, D., Leitner, A., Bieri, P., Voigts-Hoffmann, F., Erzberger, J. P., Leibundgut, M., Aebersold, R., and Ban, N. (2014) Architecture of the large subunit of the mammalian mitochondrial ribosome. *Nature 505*, 515−519.
(80) Zalk, R., Clarke, O. B., des Georges, A., Grassucci, R. A., Reiken, S., Mancia, F., Hendrickson, W. A., Frank, J., and Marks, A. R. (2015) Structure of a mammalian ryanodine receptor. *Nature 517*, 44−49.
(81) Allegretti, M., Mills, D. J., McMullan, G., Kuhlbrandt, W., and Vonck, J. (2014) Atomic model of the F420-reducing [NiFe] hydrogenase by electron cryo-microscopy using a direct electron detector. *eLife 3*, e01963.
(82) Alushin, G. M., Lander, G. C., Kellogg, E. H., Zhang, R., Baker, D., and Nogales, E. (2014) High-resolution microtubule structures reveal the structural transitions in $\alpha\beta$-tubulin upon GTP hydrolysis. *Cell 157*, 1117−1129.
(83) Amunts, A., Brown, A., Bai, X. C., Llacer, J. L., Hussain, T., Emsley, P., Long, F., Murshudov, G., Scheres, S. H., and Ramakrishnan, V. (2014) Structure of the yeast mitochondrial large ribosomal subunit. *Science 343*, 1485−1489.
(84) Bai, X. C., Fernandez, I. S., McMullan, G., and Scheres, S. H. (2013) Ribosome structures to near-atomic resolution from thirty thousand cryo-EM particles. *eLife 2*, e00461.
(85) Bartesaghi, A., Matthies, D., Banerjee, S., Merk, A., and Subramaniam, S. (2014) Structure of β-galactosidase at 3.2-Å resolution obtained by cryo-electron microscopy. *Proc. Natl. Acad. Sci. U.S.A. 111*, 11709−11714.
(86) Liao, M., Cao, E., Julius, D., and Cheng, Y. (2013) Structure of the TRPV1 ion channel determined by electron cryo-microscopy. *Nature 504*, 107−112.
(87) Lu, P., Bai, X. C., Ma, D., Xie, T., Yan, C., Sun, L., Yang, G., Zhao, Y., Zhou, R., Scheres, S. H., and Shi, Y. (2014) Three-dimensional structure of human γ-secretase. *Nature 512*, 166−170.
(88) Veesler, D., and Johnson, J. E. (2013) Cystovirus maturation at atomic resolution. *Structure 21*, 1266−1268.
(89) Veesler, D., Ng, T. S., Sendamarai, A. K., Eilers, B. J., Lawrence, C. M., Lok, S. M., Young, M. J., Johnson, J. E., and Fu, C. Y. (2013) Atomic structure of the 75 MDa extremophile *Sulfolobus* turreted icosahedral virus determined by CryoEM and X-ray crystallography. *Proc. Natl. Acad. Sci. U.S.A. 110*, 5504−5509.
(90) Wong, W., Bai, X. C., Brown, A., Fernandez, I. S., Hanssen, E., Condron, M., Tan, Y. H., Baum, J., and Scheres, S. H. (2014) Cryo-EM structure of the *Plasmodium falciparum* 80S ribosome bound to the anti-protozoan drug emetine. *eLife*, 3.
(91) Yan, Z., Bai, X. C., Yan, C., Wu, J., Li, Z., Xie, T., Peng, W., Yin, C. C., Li, X., Scheres, S. H., Shi, Y., and Yan, N. (2015) Structure of the rabbit ryanodine receptor RyR1 at near-atomic resolution. *Nature 517*, 50−55.
(92) Jain, T., Sheehan, P., Crum, J., Carragher, B., and Potter, C. S. (2012) Spotiton: A prototype for an integrated inkjet dispense and vitrification system for cryo-TEM. *J. Struct. Biol. 179*, 68−75.
(93) Langlois, R., Pallesen, J., Ash, J. T., Nam Ho, D., Rubinstein, J. L., and Frank, J. (2014) Automated particle picking for low-contrast macromolecules in cryo-electron microscopy. *J. Struct. Biol. 186*, 1−7.
(94) Scherer, S., Kowal, J., Chami, M., Dandey, V., Arheit, M., Ringler, P., and Stahlberg, H. (2014) 2dx_automator: Implementation of a semiautomatic high-throughput high-resolution cryo-electron crystallography pipeline. *J. Struct. Biol. 186*, 302−307.
(95) Murata, K., Liu, X., Danev, R., Jakana, J., Schmid, M. F., King, J., Nagayama, K., and Chiu, W. (2010) Zernike phase contrast cryo-electron microscopy and tomography for structure determination at nanometer and subnanometer resolutions. *Structure 18*, 903−912.
(96) Glaeser, R. M. (2013) Invited review article: Methods for imaging weak-phase objects in electron microscopy. *Rev. Sci. Instrum. 84*, 111101.
(97) Danev, R., Buijsse, B., Khoshouei, M., Plitzko, J. M., and Baumeister, W. (2014) Volta potential phase plate for in-focus phase contrast transmission electron microscopy. *Proc. Natl. Acad. Sci. U.S.A. 111*, 15635−15640.
(98) Russo, C. J., and Passmore, L. A. (2014) Electron microscopy. Ultrastable gold substrates for electron cryomicroscopy. *Science 346*, 1377−1380.
(99) Russo, C. J., and Passmore, L. A. (2014) Controlling protein adsorption on graphene for cryo-EM using low-energy hydrogen plasmas. *Nat. Methods 11*, 649−652.
(100) Yang, Z., Fang, J., Chittuluru, J., Asturias, F. J., and Penczek, P. A. (2012) Iterative stable alignment and clustering of 2D transmission electron microscope images. *Structure 20*, 237−247.
(101) Wang, Q., Matsui, T., Domitrovic, T., Zheng, Y., Doerschuk, P. C., and Johnson, J. E. (2013) Dynamics in cryo EM reconstructions visualized with maximum-likelihood derived variance maps. *J. Struct. Biol. 181*, 195−206.
(102) Elmlund, D., and Elmlund, H. (2012) SIMPLE: Software for ab initio reconstruction of heterogeneous single-particles. *J. Struct. Biol. 180*, 420−427.
(103) Agrawal, R. K., and Frank, J. (1999) Structural studies of the translational apparatus. *Curr. Opin. Struct. Biol. 9*, 215−221.
(104) Frank, J. (2001) Cryo-electron microscopy as an investigative tool: The ribosome as an example. *BioEssays 23*, 725−732.
(105) Stark, H. (2002) Three-dimensional electron cryomicroscopy of ribosomes. *Curr. Protein Pept. Sci. 3*, 79−91.
(106) Valle, M. (2011) Almost lost in translation. Cryo-EM of a dynamic macromolecular complex: The ribosome. *Eur. Biophys. J. 40*, 589−597.
(107) Wang, Z., Hryc, C. F., Bammes, B., Afonine, P. V., Jakana, J., Chen, D. H., Liu, X., Baker, M. L., Kao, C., Ludtke, S. J., Schmid, M. F., Adams, P. D., and Chiu, W. (2014) An atomic model of brome mosaic virus using direct electron detection and real-space optimization. *Nat. Commun. 5*, 4808.

DOI: 10.1021/acs.biochem.5b00114
Biochemistry 2015, 54, 3133−3141